2016

Synthesis and Characterization of Nanocomposite Microparticles (nCmP) for the Treatment of Cystic Fibrosis-Related Infections

Zimeng Wang

Samantha A. Meenach
University of Rhode Island, smeenach@uri.edu

Citation/Publisher Attribution
Wang, Z. & Meenach, S.A. (2016). Synthesis and Characterization of Nanocomposite Microparticles (nCmP) for the Treatment of Cystic Fibrosis-Related Infections. *Pharm Res*, *33*, 1862. doi: 10.1007/s11095-016-1921-5
Available at: http://dx.doi.org/10.1007/s11095-016-1921-5

Synthesis and Characterization of Nanocomposite Microparticles (nCmP) for the Treatment of Cystic Fibrosis-Related Infections

Zimeng Wang[1], Samantha A. Meenach[1,2]

[1]Department of Chemical Engineering, [2]Department of Biomedical and Pharmaceutical Sciences, University of Rhode Island, Kingston, RI 02881, USA

Corresponding Author: Samantha A. Meenach, Ph.D., University of Rhode Island, 202 Crawford Hall, 16 Greenhouse Road, Kingston, RI 02881. Email: smeenach@uri.edu, Phone: 401-874-4303, Fax: 401-874-4689

Running Head: "Nanocomposite Microparticles for Pulmonary Infections"

ABSTRACT

Purpose: Pulmonary antibiotic delivery is recommended as maintenance therapy for cystic fibrosis (CF) patients who experience chronic infections. However, abnormally thick and sticky mucus present in the respiratory tract of CF patients impairs mucus penetration and limits the efficacy of inhaled antibiotics. To overcome the obstacles of pulmonary antibiotic delivery, we have developed nanocomposite microparticles (nCmP) for the inhalation application of antibiotics in the form of dry powder aerosols.

Methods: Azithromycin-loaded and rapamycin-loaded polymeric nanoparticles (NP) were prepared via nanoprecipitation and nCmP were prepared by spray drying and the physicochemical characteristics were evaluated.

Results: The nanoparticles were 200 nm in diameter both before loading into and after redispersion from nCmP. The NP exhibited smooth, spherical morphology and the nCmP were corrugated spheres about 1 μm in diameter. Both drugs were successfully encapsulated into the NP and were released in a sustained manner. The NP were successfully loaded into nCmP with favorable encapsulation efficacy. All materials were stable at manufacturing and storage conditions and nCmP were in an amorphous state after spray drying. nCmP demonstrated desirable aerosol dispersion characteristics, allowing them to deposit into the deep lung regions for effective drug delivery.

Conclusions: The described nCmP have the potential to overcome mucus-limited pulmonary delivery of antibiotics.

KEYWORDS

Nanocomposite microparticles, pulmonary delivery, cystic fibrosis, spray drying

ABBREVIATIONS

Cystic fibrosis (CF), cystic fibrosis transmembrane conductance regulator (CFTR), nanoparticles (NP), nanocomposite microparticles (nCmP), azithromycin (AZI), rapamycin (RAP), acetalated dextran (Ac-Dex), poly(ethylene glycol) vitamin E (VP5k), p-toluenesulfonate (PPTS), poly(ethylene glycol) methyl ether (mPEG), N,N'-dicyclohexyl- carbodiimde (DCC), 4-(dimethylamino) pyridine (DMAP), 2-methoxypropene (2-MOP), triethylamine (TEA), deuterium chloride (DCl), deuterated chloroform ($CDCl_3$), deuterium oxide (D_2O), cyclic-to-acyclic (CAC), powder X-ray diffraction (PXRD), Karl Fischer (KF), Next Generation Impactor (NGI), hydroxypropyl methylcellulose (HPMC), fine particle dose (FPD), fine particles fraction (FPF), respirable fraction (RF), emitted dose (ED), encapsulation efficiency (EE)

INTRODUCTION

Cystic fibrosis (CF) is a progressive, incurable, autosomal recessive disease that affects around 70,000 people worldwide (1, 2). It is caused by mutations in the cystic fibrosis transmembrane conductance regulator (CFTR) gene, which leads to defective or insufficient amounts of functional CFTR proteins. The dysfunctional proteins result in an absence or decrease of chloride in secretions, leading to increased sodium and water absorption and airway surface liquid depletion (3). CF affects various organ systems of patients including the sweat glands,

reproductive tract, intestine, liver, pancreas, and respiratory tract (4), in which lung disease is the primary cause of mortality (4, 5). The dysfunction of the respiratory tract results in frequent pulmonary infections, inflammation, bronchiectasis, and eventually respiratory failure, which causes over 90% of deaths in CF patients (6). Pulmonary infection is one of the primary complications among patients with CF and these patients tend to develop chronic infections within a year if no treatment is implemented, which will accelerate the decline in lung function, resulting in earlier mortality (7, 8).

Pseudomonas aeruginosa (*P. aeruginosa*) is regarded as the most prevalent pathogen in CF patients' lungs (7, 9). Azithromycin (AZI) is a macrolide antibiotic with a broad gram-negative antibacterial spectrum and is highly effective against planktonic, actively growing bacteria (10). AZI has been extensively studied for the treatment of CF-related infections due to its ability to decrease *P. aeruginosa* accumulation (10-15) as well as its pharmacokinetic advantages including high bioavailability, distribution, and extended half-life (13, 14).

Burkholderia cenocepacia (*B. cepacia*) infection is also considered to be a lethal threat to CF patients because it causes severe and persistent lung inflammation and it is resistant to nearly all available antibiotics (16). Rapamycin (RAP), also known as sirolimus, is an immunosuppressive macrolide that is the most commonly used chemical to induce autophagy (17). It has been shown that RAP can markedly decrease *B. cepacia* infection *in vitro* by enhancing the clearance of this bacterium via induced autophagy. RAP has been shown to reduce bacterial burden and decrease inflammation in the lungs of CF infected mice (16).

Acetalated dextran (Ac-Dex) is an acid sensitive, biodegradable, biocompatible polymer that can be prepared in a one-step reaction by reversibly modifying dextran with acetal groups (18). This modification reverses the solubility properties of dextran from hydrophilic to hydrophobic, making it possible to form polymeric particles using standard emulsion or nanoprecipitation techniques. Drug loaded Ac-Dex nanoparticles exhibit sustained release profile, with the advantages of extended duration of action, decreased drug use, improved management of therapy, enhanced compliance and reduced side effects. (19, 20) In comparison to other commonly used polymers in drug delivery such as poly(lactic-co-glycolic acid) (PLGA) and polyesters, Ac-Dex offers several advantages. Most notably, the degradation rate of Ac-Dex can be tuned from minutes to months by modifying the ratio of cyclic and acyclic acetal groups, which have different rates of hydrolysis. Also, Ac-Dex degrades into dextran, a biocompatible, biodegradable, FDA-approved by-product, and very low levels of methanol and acetone (20-22).

Mannitol, an FDA approved, non-toxic, readily degradable sugar alcohol commonly used in pharmaceutical products, was applied as the excipient of nCmP due to its beneficial properties.(23) First, mannitol can be rapidly dissolved into an aqueous environment, leading to a burst release of encapsulated nanoparticles. In addition, mannitol can improve the fluidity of mucus, thus enhancing the mucus penetration rate of nanoparticles (24). Mannitol has been extensively studied as a carrier in spray-dried powder aerosols for pulmonary drug administration and the resulting particles have been shown to exhibit desirable water content, size, and surface morphology for successful aerosol delivery (25, 26).

Pulmonary antibiotic delivery is increasingly recommended as maintenance therapy to prolong the interval between pulmonary exacerbations and to slow the progression of lung disease of CF patients due to the capability of these systems to achieve high drug concentrations at the site of infection and to minimize the risk of systemic toxicity and drug resistance (31-34). Extensive studies have been devoted to the development of new inhalation devices and advanced drug delivery formulations for the treatment of CF-related infections (35-38). Despite these advances, there has only been incremental improvement in the treatment of pulmonary infections. This is partly due to the presence of mucus in the lung airways that can trap and remove foreign particles. Also, the abnormally thick and viscous mucus in the respiratory tract of CF patients impairs efficient mucus penetration and limits the efficacy of antibiotics delivered via inhalation. Polyethylene glycol (PEG)-coated nanoparticles have been shown to significantly improve the mucus penetration of various therapeutics encapsulated in NP due to the formulation size, PEG coating, and protection of active pharmaceutical ingredients (39). Unfortunately, aerosolized nanoparticles will be exhaled owing to their small size and mass and while aerosolized particles with aerodynamic diameters of 1-5 μm can deposit into the deep lung region, which limits their efficacy for targeting the infection site in mucus as aerosol drug delivery vehicles (40, 41).

To overcome the aforementioned obstacles of pulmonary antibiotic delivery, we developed nanocomposite microparticles (nCmP) in the form of dry powder aerosols (**Figure 1**). This system is comprised of drug-loaded nanoparticles (NP) entrapped in microparticle carriers with the excipient mannitol to allow for the delivery of mucus-penetrating NP to the lungs. The

141 drug-loaded nanoparticles contain azithromycin or rapamycin as model drugs and are coated by a
142 vitamin E poly(ethylene glycol) (MW 5000) layer, which has shown to improve the stability and
143 mucus penetration rate of nanoparticles (39). Upon pulmonary administration, the nCmP will
144 deposit on the mucus in the respiratory tract, dissociate into free NP and mannitol, and allow the
145 nanoparticles to penetrate the mucus and then release drug to the targeted site at sustained rate.
146 This nCmP system exhibits features favorable for dry powder-based antibiotic delivery including
147 targeted delivery, rapid mucus penetration, and controlled drug release. The goal of the described
148 research was the initial development and physicochemical characterization of the nCmP systems
149 via particle engineering.

150

151 **MATERIALS AND METHODS**

152 **Materials**

153 Dextran from *Leuconostoc mesenteroides* (9000 - 11000 MW), pyridinium
154 p-toluenesulfonate (PPTS, 98%), poly(ethylene glycol) methyl ether (mPEG, Mn 5000), D-α
155 -tocopherol succinate (vitamin E succinate, 1210 IU/g), N,N'-dicyclohexyl- carbodiimde (DCC,
156 99%), 4-(dimethylamino) pyridine (DMAP, ≥ 99%), potassium phosphate dibasic, potassium
157 phosphate monobasic, D-mannitol (≥ 98%), 2-methoxypropene (2-MOP, 97%), triethylamine
158 (TEA, ≥ 99%), anhydrous dimethyl sulfoxide (DMSO, ≥ 99.9%), deuterium chloride (DCl, 35
159 weight % in D_2O, 99 atom % D), deuterated chloroform ($CDCl_3$, 100%, 99.96 atom % D),
160 TWEEN® 80, methanol (HPLC grade, ≥ 99.9%), and acetonitrile (HPLC grade, ≥ 99.9%)

were obtained from Sigma–Aldrich (St. Louis, MO). Ethanol (anhydrous, ASC/USP grade) was obtained from Pharmco-AAPER (Brookfield, CT). Deuterium oxide (D_2O, 99.8% atom D) was obtained from Acros Organics (Geel, Belgium). Phosphate buffered saline (PBS) was obtained from Fisher Scientific. Hydranal® KF reagent was obtained from Fluka Analytical. Rapamycin was obtained from LC Laboratories (Woburn, MA). Azithromycin was obtained from AstaTech Inc. (Bristol, PA).

Synthesis of Acetalated Dextran (Ac-Dex)

Ac-Dex was synthesized as described previously (22) with minor modifications. Briefly, 1 g of lyophilized dextran and 25 mg of PPTS were dissolved in 10 mL anhydrous DMSO. The resulting solution was reacted with 5 mL of 2-MOP under nitrogen gas for 5 minutes and was quenched with 1 mL of TEA. The reaction mixture was then precipitated in basic water (water and TEA, pH 9), vacuum filtered, and lyophilized (−50 °C, 0.023 mbar) for 24 hours to yield a solid product.

Synthesis of Vitamin E Poly(ethylene glycol) (VP5k)

VP5k was prepared with some modifications to a previously described method (42). 0.65 g of vitamin E succinate and 7.334 g of mPEG were dissolved in 20 mL of DCM. 0.278 g of DCC and 15 mg of DMAP were added to the solution. The reaction mixture was stirred at room temperature overnight, vacuum filtered (0.45 μm), and concentrated under reduced pressure via a rotor evaporator (IKA-RV, Wilmington, NC) to obtain a crude product. The resulting crude

product was dissolved at 5% (w/v) in DI water and centrifuged at 12000 rpm for 30 minutes. The filtrate was vacuum filtered (0.22 μm) and lyophilized (−50 °C, 0.023 mbar) for 72 hours to yield the final product.

NMR Analysis of Ac-DEX and VP5k

The cyclic-to-acyclic (CAC) ratio of acetal coverage and degrees of total acetal coverage per 100 glucose molecules was confirmed by ^{1}H NMR spectroscopy (Bruker 300 MHz NMR, MA). 10 mg of Ac-Dex was added to 700 μL of D_2O and was hydrolyzed with 30 μL of DCl prior to analysis. The hydrolysis of one cyclic acetal group produces one acetone whereas one acyclic acetal produces one acetone and one methanol. Consequently, from the normalized integrations of peaks related to acetone, methanol, and the carbon ring of dextran, the CAC ratio of acetal coverage and degrees of total acetal coverage per 100 glucoses were determined.

Conjugation of mPEG to Vitamin E succinate was also confirmed by NMR spectroscopy. 20 mg of VP5k was dissolved in 600 μL of $CDCl_3$. The resulting solution was analyzed by 2D 1H-13C HMBC-GP NMR spectroscopy. Shift of the signal at 2.8 ppm and 178.8 ppm related to the -COOH group of vitamin E succinate and 2.7 ppm and 172.2 ppm related to the ester group indicated conjugation of mPEG to vitamin E succinate for the successful formation of VP5k.

Preparation of Drug-loaded Nanoparticles

Azithromycin (AZI)-loaded nanoparticles and rapamycin (RAP)-loaded nanoparticles were prepared via nanoprecipitation. 40 mg of Ac-Dex and 12 mg of AZI or 4 mg of RAP were

dissolved in 1 mL of ethanol and injected into 40 mL of 1.5 % (w/v) VP5k solution. The resulting suspension was stirred for 3 hours for removal of ethanol and hardening of the particles and the final solution was centrifuged at 12000 rpm for 20 minutes to collect the NP. The NP were washed once with basic water and lyophilized for 24 hours to give the final AZI-NP and RAP-NP systems.

Preparation of Nanocomposite Microparticles (nCmP)

nCmP were prepared via the spray drying of a AZI NP or RAP NP suspensions and mannitol in an aqueous solution using a Büchi B-290 spray dryer (Büchi Labortechnik, AG, Switzerland) in open mode. The spray drying conditions were as follows: 1:1 (w:w) ratio of NP to mannitol in DI water; feed solution concentration of 1% (w/v); 1.4 mm nozzle diameter; atomization gas flow rate of 414 L/h (UHP dry nitrogen); aspiration rate of 28 m^3/h, inlet temperature of 50 °C; pump rate of 0.6 mL/min; and nozzle cleaner rate of 4. The resulting nCmP were separated in a high-performance cyclone, collected in a sample collector, and stored in amber glass vials in desiccators at −20°C.

Powder X-Ray Diffraction (PXRD)

Crystalline states of the nCmP were examined by PXRD using a Rigaku Multiflex X-ray diffractometer (The Woodlands, TX) with a Cu Kα radiation source (40 kV, 44 mA). The samples were placed on a horizontal quartz glass sample holder (3 mm). The scan range was 5 – 65° in 2Θ with a step width of 0.02 and scan rate of 2°/min.

224

225 **Differential Scanning Calorimetry (DSC)**

226 The thermal phase transitions of the nCmP were determined by DSC using a TA Q200 DSC
227 system (TA Instruments, New Castle, DE, USA) equipped with an automated
228 computer-controlled RSC-90 cooling accessory. 1 - 3 mg of sample was weighed into Tzero™
229 alodined aluminum pans that were hermetically sealed. The sealed pans were placed into the
230 DSC furnace along with an empty sealed reference pan. The heating range was 0 – 250 °C at a
231 heating rate of 10 °C/min.

232

233 **Scanning Electron Microscopy (SEM)**

234 The shape and surface morphology of the NP and nCmP were evaluated by SEM using a
235 Hitachi S-4300 microscope (Tokyo, Japan). nCmP samples were placed on aluminum SEM stubs
236 (TedPella, Inc., Redding, CA, USA) with double-sided adhesive carbon tabs. Nanoparticles were
237 dispersed in basic water (pH = 9, 10 mg/mL) and this suspension was dropped onto aluminum
238 SEM stubs and then dried at room temperature. Both the NP and nCmP samples were coated
239 with a thin film of a gold/palladium alloy using an Emscope SC400 sputter coating system at 20
240 μA for 75 seconds under argon gas. Images were captured at 5 kV.

241

242 **Particle Size, Size Distribution and Zeta Potential Analysis**

243 The size, size distribution, and zeta potential of the NP systems were measured by dynamic
244 light scattering (DLS) using a Malvern Nano Zetasizer (Malvern Instruments, Worcestershire,

UK). The NP were dispersed in basic water (pH = 9, 0.3 mg/mL). All experiments were performed in triplicate with a scattering angle of 173° at 25 °C. The mean size and standard deviation of the nCmP were measured digitally from SEM images using ImageJ software (Systat, San Jose, CA, USA). Representative micrographs (5k magnification) for each sample were analyzed by measuring the diameter of at least 100 particles.

Karl Fischer (KF) Titration

The water content of the nCmP was quantified by Karl Fischer (KF) titration using a 737 KF coulometer (Metrohm, Riverview, FL). Approximately 10 mg of powder was dissolved in anhydrous methanol. The resulting solution was injected into the KF reaction cell filled with Hydranal® KF reagent and then the amount of water was analyzed. Pure solvent was also injected for use as a background sample.

Aerosol Dispersion Analysis

In vitro aerosol dispersion performance of the nCmP was evaluated using a Next Generation Impactor™ (NGI™, MSP Corporation, Shoreview, MN) equipped with a stainless steel induction port (USP throat adaptor) attachment and stainless steel NGI™ gravimetric insert cups. The NGI™ was coupled with a Copley TPK 2000 critical flow controller, which was connected to a Copley HCP5 vacuum pump (Copley Scientific, United Kingdom). The airflow rate (Q) was measured and adjusted to 60 L/min in order to model the flow rate in a healthy adult lung before each experiment. Glass fiber filters (55 mm, Type A/E, Pall Life Sciences, PA) were placed in

266 the gravimetric insert cups for stages 1 through 7 to minimize bounce or re-entrapment (43) and
267 these filters were weighed before and after the experiment to determine the particle mass
268 deposited on each stage. Approximately 10 mg of powder was loaded into a hydroxypropyl
269 methylcellulose (HPMC, size 3, Quali-V®, Qualicaps® Inc., Whitsett, NC, USA) capsule and
270 the capsule was placed into a human dry powder inhaler device (HandiHaler, Boehringer
271 Ingelheim Pharmaceuticals, CT) attached to a customized rubber mouthpiece connected to the
272 NGI™. Three HPMC capsules were loaded and released in each measurement and experiments
273 were performed in triplicate. The NGI™ was run with a delay time of 10 s and running time of
274 10 s. For Q = 60 L/min, the effective cutoff diameters for each stage of the impactor were given
275 from the manufacturer as: stage 1 (8.06 μm); stage 2 (4.46 μm); stage 3 (2.82 μm); stage 4 (1.66
276 μm); stage 5 (0.94 μm); stage 6 (0.55 μm); and stage 7 (0.34 μm). The fine particle dose (FPD),
277 fine particle fraction (FPF), respirable fraction (RF), and emitted dose (ED) were calculated as
278 follows:
279

$$\text{Fine particles dose (FPD)} = \text{mass of particles on Stages 2 through 7}$$

$$\text{Fine particles fraction (FPF)} = \frac{\text{fine particles dose}}{\text{initial particle mass loaded into capsules}} \times 100\%$$

280

$$\text{Respirable fraction (RF)} = \frac{\text{mass of particles on Stages 2 through 7}}{\text{total particle mass on all stages}} \times 100\%$$

$$\text{Emitted dose (ED)} = \frac{\text{initial mass in capsules - final mass remaining in capsules}}{\text{initial mass in capsules}} \times 100\%$$

281

The mass median aerodynamic diameter (MMAD) and geometric standard deviation (GSD) for the particles were determined using a Mathematica® program written by Dr. Warren Finlay (43, 44).

Analysis of Nanoparticle Drug Loading and Nanoparticle Loading in nCmP

Drug loading and encapsulation efficacy of AZI and RAP NP and nCmP were determined using high performance liquid chromatograph (HPLC) (Hitachi Elite LaChrom, Japan). Detection of AZI was performed using the following conditions: C_{18}, 5 μm × 150 mm × 4.6 mm column (XTerra™, Waters); 1.5 mL/min pump rate; 6 minute retention time; mobile phase of 70% methanol and 30% PBS (0.03 M, pH = 7.4); absorbance of 215 nm; and ambient temperature. Detection of RAP was performed using following conditions: C_{18}, 5 μm × 150 mm × 4.6 mm column (Supelco, Sigma-Aldrich, St. Louis, MO); 1 mL/min pump rate; 6 minute retention time; mobile phase of 65% acetonitrile and 35% DI water; absorbance of 278 nm; and temperature of 50°C. Drug-loaded NP and nCmP were fully dissolved in their respective mobile phases. The experimental drug concentration in each sample was quantified by comparison with a standard curve of drug in its mobile phase. The drug loading of NP, drug loading of nCmP, NP loading in nCmP, drug encapsulation efficiency of NP, and NP encapsulation efficacy in nCmP were determined by the following equations:

$$\text{Drug loading} = \frac{\text{mass of drug loaded in nanoparticles}}{\text{mass of particles}} \times 100\%$$

$$\text{Drug encapsulation efficacy (EE)} = \frac{\text{mass of drug loaded in nanoparticles}}{\text{initial mass of drug in particle formulation}} \times 100\%$$

$$\text{Nanoparticles loading} = \frac{\text{mass of NPs loaded in nCmPs}}{\text{mass of nCmPs}} \times 100\%$$

$$\text{NP loading efficacy} = \frac{\text{mass of NPs loaded in nCmPs}}{\text{initial mass of NPs in nCmPs formulation}} \times 100\%$$

In Vitro Drug Release from Nanoparticles

The *in vitro* release profiles of AZI or RAP from nanoparticles was determined via a release study of NP suspended (1 mg/mL) in modified phosphate buffer (0.1 M, pH = 7.4) with 0.2% (w/v) of Tween® 80. The suspension was incubated at 37 °C and 100 rpm. At various time points (0 to 48 h), NP samples were centrifuged at 14000 rpm for 5 minutes at 4 °C to isolate the NP. 200 μL of supernatant was withdrawn and replaced by the same amount of fresh modified PBS in each sample. The withdrawn solutions were analyzed for drug content via HPLC using the same methods described in the previous section.

Statistical analysis

All measurements were performed in at least triplicate. Values are given in the form of means ± SD. The statistical significance of the results was determined using t-Test. A p-value of <0.05 was considered statistically significant.

RESULTS AND DISCUSSION

NMR Analysis of Ac-Dex and VP5k

Successful synthesis of Ac-Dex and VP5k was confirmed by NMR (**Figure S1** in Supplemental Information). Ac-Dex exhibited 68.7% cyclic acetal coverage (CAC) and 79.1% total acetal coverage (conversion of -OH groups). A yield of approximately 95% was obtained for this Ac-Dex. An increase in CAC is known to slow drug release due to slower degradation.(21, 22) A high total acetal coverage (higher than 75% according to our research) is required to stabilize the VP5k coating of nanoparticles, which ensures small particles size and narrow size distribution. The signals for ester groups were detected via NMR, indicating successful conjugation of mPEG to vitamin E succinate for the successful formation of VP5k (45). The yield of VP5k was approximately 30%.

Characterization of Nanoparticles

The azithromycin-loaded nanoparticles (AZI-NP), shown in **Figure 2A**, appear as uniform spheres with smooth surface morphology. NP size, size distribution, and zeta potential are shown in **Table 1**. The resulting sizes of the NP analyzed via DLS (approximately 200 nm) were larger than those observed from SEM micrographs and ImageJ analysis (approximately 100 nm) due to shrinking of the particles during freeze-drying from the collapse of hydrated PEGylated chains (46). Both drug-loaded NP systems exhibited desirable size (less than 200 nm) with narrow size distribution to allow for potential mucus penetration. The relative surface charge of the NP systems were nearly neutral, confirming PEG coverage on their surfaces (45). Similar results

were obtained for drug-loaded and blank nanoparticles with respect to their size, size distribution, and surface charge, indicating that drug encapsulation did not affect the formation of the NP.

Both AZI and RAP were successfully encapsulated into the described NP systems. 13.0 % of initial AZI and 25.8 % of initial RAP were effectively entrapped within the NP prepared using nanoprecipitation of Ac-Dex and drugs in VP5k solution. The low encapsulation of the drugs may be due to the improved solubility of the drugs in the spinning solution by VP5K micelles. RAP-NP exhibited a higher encapsulation efficacy as a result of the lower solubility of RAP than AZI in the aqueous spinning solution.

Results of the *in vitro* release of AZI-NP and RAP-NP at physiological pH and temperature are reported in **Figure 3** as the percentage of drug released over time. Both NP systems displayed sustained release for approximately 12 hours, which matched the degradation profile of other Ac-Dex particle systems (43). Based on previous research, Ac-Dex made of 10kDa dextran and reacted for 5 minutes showed a maximum of degradation at 6 hours and negligible degradation after that (47). A possible explanation of the release profiles could be that the first release stage corresponds to Ac-Dex degradation as well as nanoparticle dissociation, whereas after 6 hours the rate of drug release is controlled by drugs passively diffuse out of the dissociated matrix of nanoparticles following the partial degradation of Ac-Dex.

Manufacturing of nCmP

With respect to nCmP manufacturing, the outlet temperatures of AZI- and RAP-nCmP were

30 - 31 °C and 30 - 33 °C, respectively, while the yields were 62.4% and 60.6%, respectively.

nCmP Morphology, Sizing, and Size Distribution

As seen in the SEM images, the AZI-nCmP were mostly spherical with a corrugated surface (**Figure 2B**) and encapsulated nanoparticles were visible on the surface of the nCmP as seen in **Figure 2C**. Both RAP-NP and RAP-nCmP exhibited the same morphology as the AZI loaded systems (data not shown). The number average geometric diameters were 1.03 ± 0.46 and 1.12 ± 0.43 μm for AZI-nCmP and RAP-nCmP, respectively, as determined by ImageJ analysis. Both nCmP systems exhibited similar morphology, geometric size, and size distribution due to the similarities in spray drying conditions.

Karl Fisher (KF) Titration

The residual water contents of AZI-nCmP and RAP-nCmP were approximately 6% (**Table 2**). This is within the range of other nCmP in our group (results not published) and that of previously reported inhalable dry powder formulations prepared by other groups (25, 48-51). Water in inhalable powders can significantly reduce their dispersion properties during aerosolization due to the interparticulate capillary forces acting at the solid–solid interface between particles (52) and also have a negative effect on the stability of the powders (50). Correspondingly, low water content in the powder is highly favorable for efficient dry powder aerosolization and effective particle delivery (52, 53).

Differential Scanning Calorimetry (DSC)

Figure 4 shows DSC thermograms of the raw materials used in particle preparation and the final drug-loaded nCmP. Raw Ac-Dex, AZI, RAP, and mannitol displayed endothermic main phase transition peaks (T_m) near 170, 140, 180, and 170 °C respectively, which are in accordance with previously reported values (54-56). The drug-loaded nCmP systems exhibited similar thermal behaviors with a main phase transition peak near 165 °C corresponding to the melting of Ac-Dex and mannitol. This melting point was lower than those of raw Ac-Dex and mannitol, indicating an increase in the amorphous state of these raw materials in nCmP. No glass transition or other phase transitions were present under 120 °C, which indicated that all the materials will be stable during manufacturing and storage.

Powder X-ray Diffraction (PXRD)

X-ray diffraction diffractograms of the raw materials and drug-loaded nCmP are shown in **Figure 5**. Strong peaks were present for raw AZI, RAP, and mannitol powders. These strong peaks indicate that the raw materials are in their crystalline forms prior to spray drying, which is in accordance with previous research (54-56). No strong peaks were present for raw Ac-Dex, indicating that it is non-crystalline. This is quite different from commercialized polymers such as PLGA, which exhibits strong XRD characterization peaks (54-57). The absence of diffraction peaks in Ac-Dex is likely because the Ac-Dex is collected by rapid precipitation in water. XRD patterns of AZI-nCmP and RAP-nCmP showed the absence of any diffraction peaks, suggesting amorphization of raw AZI and RAP in the particle matrix. Also, the peaks characterizing

401 mannitol were significantly reduced, indicating that mannitol is primarily in an amorphous state
402 in the nCmP. The results obtained from the XRD diffractograms confirmed those from DSC
403 thermograms, where raw AZI, RAP, and mannitol were converted into amorphous form in the
404 nCmP manufacturing process.
405
406 **Drug and Nanoparticles Loading in nCmP**
407 HPLC was used to determine the amount of drug loading in nCmP, which can be used to
408 calculate the resulting nanoparticles loading and nanoparticle encapsulation efficacy in nCmP.
409 These results are shown in **Table 2**. Both AZI- and RAP-nCmP exhibited desirable drug loading,
410 high nanoparticle loading, and nanoparticle encapsulation efficacy. In addition, standard
411 deviations of these three values were very low, which indicated reproducible drug loading of the
412 nCmP can be achieved.
413
414 **Nanoparticle Redispersion from nCmP**
415 The properties of NP redispersed from nCmP were evaluated using DLS (**Table S1** in
416 Supplementary Material). The size and size distribution of the NP increased after redispersion,
417 which is likely a result of agglomeration that occurred during spray drying. The NP surface
418 charges remained neutral due to the presence of PEG on the surface of the NP. These parameters
419 were all within the desirable ranges for effective mucus penetration.
420
421 ***In vitro* Aerosol Performance of nCmP**

In vitro aerosol dispersion performance properties (**Figure 6** and **Table 2**) of the nCmP were evaluated using a Next Generation Impactor™ coupled with a human DPI device. The results indicated that the formulated nCmP are favorable for efficient dry powder aerosolization and effective targeted delivery. The MMAD values of AZI-nCmP and RAP-nCmP were 3.93 ± 0.09 and 3.86 ± 0.07 μm, while the GSD values were 1.73 ± 0.06 and 1.78 ± 0.06 μm, respectively. The MMAD values were within the range of 1 - 5 μm, which is required for predominant deposition of nCmP into the deep lung region where infection persists (49). The GSD values were within those previously reported and the RF, FPF, and ED values were all higher (43, 49, 58). Assuming that nCmP drug loading is homogenous, fine particle doses in terms of drug mass of AZI-nCmP and RAP-nCmP are 110.42 ± 0.22 μg and 100.97 ± 9.19 μg. There is no research on the therapeutic level of rapamycin for the treatment of CF-related infection. Oral delivery of azithromycin requires 500 mg/week to 1500 mg/ week, but the bioavailability is limited.(13) The nCmP system is expected to achieve therapeutic effect using a low drug amount by improving the delivery efficacy. 8.1% and 9.4% of AZI-nCmP and RAP-nCmP deposited on stages 5 - 7, respectively, and are predicted to deposit in the deep lung alveolar region due to diffusion mechanisms (59) of deposition, while approximate 84% of both the nCmP deposited on stages 2 - 4, and are predicted to deposit predominantly in the deep lung regions by sedimentation due to gravitational settling (60-62). Overall, the nCmP exhibited desirable aerosol dispersion characteristics allowing them to deposit in deep lung regions for drug delivery.

Summary

Both nCmP systems exhibited similar morphology, geometric size, size distribution, water content, drug loading, nanoparticles loading, and nanoparticle encapsulation efficacy as well as outlet temperature and yield due to the fact that they were prepared with nanoparticles with the same spray drying conditions.

CONCLUSIONS

Both azithromycin and rapamycin were successfully encapsulated in Ac-Dex nanoparticles and can be released in a sustained rate. The drug-loaded nanoparticles were smooth spheres 200 nm in diameter with narrow size distribution and slightly negative surface charge, which is desirable for mucus penetration. Most nanoparticles maintained these properties during the nCmP manufacturing process as shown in redispersion testing. The nCmP systems were corrugated spheres of 1 μm with observable nanoparticles present on their surfaces. The water content of the nCmP systems was relatively low, which can enable efficient dry powder aerosolization and particle delivery. None of the raw materials underwent degradation during nCmP manufacturing, indicating the stability of the therapeutics during formation. No crystalline structures of AZI and RAP were observed in the nCmP, which confirmed that both drugs in the nCmP were in their amorphous form. *In vitro* aerosol performance testing demonstrated desirable aerosol dispersion characteristics of nCmP, allowing them to deposit in deep lung regions for drug delivery.

This nCmP system sheds a light on dry powder-based antibiotic delivery due to its novel

features including targeted pulmonary delivery, rapid mucus penetration potential, and controlled drug release. It can be applied as a promising alternative of the traditional antibiotic treatment by providing effective delivery of therapeutics, more convenient administration, more flexible storage conditions, and lower risk of contamination in the device.

ACKNOWLEDGEMENTS

The authors gratefully acknowledge financial support from an Institutional Development Award (IDeA) from the National Institute of General Medical Sciences of the National Institutes of Health under grant number P20GM103430. The content is solely the responsibility of the authors and does not necessarily represent the official views of the National Institutes of Health. The authors thank RI-INBRE for HPLC access and RIN2 for SEM, DLS, PXRD, and DSC access.

REFERENCES

1. S.-J. Bowenand J. Hull. The basic science of cystic fibrosis. Paediatrics and Child Health. 25:159-164 (2015).
2. N.A. Bradbury. Cystic Fibrosis, Academic Press2016.
3. R.M. Thursfieldand J.C. Davies. Cystic Fibrosis: therapies targeting specific gene defects. Paediatric Respiratory Reviews. 13:215-219 (2012).
4. A. Chuchalin, E. Amelina, and F. Bianco. Tobramycin for inhalation in cystic fibrosis: Beyond respiratory improvements. Pulmonary Pharmacology & Therapeutics. 22:526-532 (2009).
5. C.E. Milla. Nutrition and Lung Disease in Cystic Fibrosis. Clinics in Chest Medicine. 28:319-330 (2007).
6. C. FibrosisFoundation. Patient Registry 2005 Annual Report, Bethesda, Maryland, 2005.

7. H. Heijerman, E. Westerman, S. Conway, and D. Touw. Inhaled medication and inhalation devices for lung disease in patients with cystic fibrosis: A European consensus. Journal of Cystic Fibrosis. 8:295-315 (2009).
8. R. Sand S. L. Pulmonary infections in patients with cystic fibrosis. Seminars in Respiratory Infections 17:47-56 (2002).
9. W.E. Regelmann, G.R. Elliott, W.J. Warwick, and C.C. Clawson. Reduction of Sputum Pseudomonas aeruginosa Density by Antibiotics Improves Lung Function in Cystic Fibrosis More than Do Bronchodilators and Chest Physiotherapy Alone. American Review of Respiratory Disease. 141:914-921 (1990).
10. T. Wagner, G. Soong, S. Sokol, L. Saiman, and A. Prince. EFfects of azithromycin on clinical isolates of pseudomonas aeruginosa from cystic fibrosis patients*. Chest. 128:912-919 (2005).
11. K.W. Southernand P.M. Barker. Azithromycin for cystic fibrosis. European Respiratory Journal. 24:834-838 (2004).
12. L. Saiman, B.C. Marshall, N. Mayer-Hamblett, and et al. Azithromycin in patients with cystic fibrosis chronically infected with pseudomonas aeruginosa: A randomized controlled trial. JAMA. 290:1749-1756 (2003).
13. E.B. Wilms, D.J. Touw, H.G.M. Heijerman, and C.K. van der Ent. Azithromycin maintenance therapy in patients with cystic fibrosis: A dose advice based on a review of pharmacokinetics, efficacy, and side effects. Pediatric Pulmonology. 47:658-665 (2012).
14. P. SC, D. LH, and R. KA. Clarithromycin and azithromycin: new macrolide antibiotics. Clinical Pharmacology. 11:137-152 (1992).
15. M. Zhao, Y. You, Y. Ren, Y. Zhang, and X. Tang. Formulation, characteristics and aerosolization performance of azithromycin DPI prepared by spray-drying. Powder Technology. 187:214-221 (2008).
16. B.A. Abdulrahman, A.A. Khweek, A. Akhter, K. Caution, S. Kotrange, D.H.A. Abdelaziz, C. Newland, R. Rosales-Reyes, B. Kopp, K. McCoy, R. Montione, L.S. Schlesinger, M.A. Gavrilin, M.D. Wewers, M.A. Valvano, and A.O. Amer. Autophagy stimulation by rapamycin suppresses lung inflammation and infection by Burkholderia cenocepacia in a model of cystic fibrosis. Autophagy. 7:1359-1370 (2011).
17. Y.-C. Chen, C.-L. Lo, Y.-F. Lin, and G.-H. Hsiue. Rapamycin encapsulated in dual-responsive micelles for cancer therapy. Biomaterials. 34:1115-1127 (2013).
18. K.E. Broaders, J.A. Cohen, T.T. Beaudette, E.M. Bachelder, and J.M.J. Frechet. Acetalated dextran is a chemically and biologically tunable material for particulate immunotherapy. Proceedings of the National Academy of Sciences of the United States of America. 106:5497-5502 (2009).
19. R.O. Cook, R.K. Pannu, and I.W. Kellaway. Novel sustained release microspheres for pulmonary drug delivery. J Control Release. 104:79-90 (2005).
20. K.J. Kauffman, N. Kanthamneni, S.A. Meenach, B.C. Pierson, E.M. Bachelder, and K.M. Ainslie. Optimization of rapamycin-loaded acetalated dextran microparticles for immunosuppression. International Journal of Pharmaceutics. 422:356-363 (2012).

21. K.E. Broaders, J.A. Cohen, T.T. Beaudette, E.M. Bachelder, and J.M.J. Fréchet. Acetalated dextran is a chemically and biologically tunable material for particulate immunotherapy. Proceedings of the National Academy of Sciences. 106:5497-5502 (2009).
22. E.M. Bachelder, T.T. Beaudette, K.E. Broaders, J. Dashe, and J.M.J. Fréchet. Acetal-Derivatized Dextran: An Acid-Responsive Biodegradable Material for Therapeutic Applications. Journal of the American Chemical Society. 130:10494-10495 (2008).
23. J.O.H. Sham, Y. Zhang, W.H. Finlay, W.H. Roa, and R. Löbenberg. Formulation and characterization of spray-dried powders containing nanoparticles for aerosol delivery to the lung. International Journal of Pharmaceutics. 269:457-467 (2004).
24. H.X. Ong, D. Traini, G. Ballerin, L. Morgan, L. Buddle, S. Scalia, and P.M. Young. Combined Inhaled Salbutamol and Mannitol Therapy for Mucus Hyper-secretion in Pulmonary Diseases. Aaps J. 16:269-280 (2014).
25. D.M.K. Jensen, D. Cun, M.J. Maltesen, S. Frokjaer, H.M. Nielsen, and C. Foged. Spray drying of siRNA-containing PLGA nanoparticles intended for inhalation. J Control Release. 142:138-145 (2010).
26. E.M. Littringer, A. Mescher, H. Schroettner, L. Achelis, P. Walzel, and N.A. Urbanetz. Spray dried mannitol carrier particles with tailored surface properties – The influence of carrier surface roughness and shape. European Journal of Pharmaceutics and Biopharmaceutics. 82:194-204 (2012).
27. W. Kaialy, H. Larhrib, G. Martin, and A. Nokhodchi. The Effect of Engineered Mannitol-Lactose Mixture on Dry Powder Inhaler Performance. Pharm Res. 29:2139-2156 (2012).
28. K. Kramek-Romanowska, M. Odziomek, T.R. Sosnowski, and L. Gradoń. Effects of Process Variables on the Properties of Spray-Dried Mannitol and Mannitol/Disodium Cromoglycate Powders Suitable for Drug Delivery by Inhalation. Industrial & Engineering Chemistry Research. 50:13922-13931 (2011).
29. E.M. Littringer, R. Paus, A. Mescher, H. Schroettner, P. Walzel, and N.A. Urbanetz. The morphology of spray dried mannitol particles — The vital importance of droplet size. Powder Technology. 239:162-174 (2013).
30. T.F. Guimarães, A.D. Lanchote, J.S. da Costa, A.L. Viçosa, and L.A.P. de Freitas. A multivariate approach applied to quality on particle engineering of spray-dried mannitol. Advanced Powder Technology. 26:1094-1101 (2015).
31. G.F. Cooney, B.L. Lum, M. Tomaselli, and S.B. Fiel. Absolute Bioavailability and Absorption Characteristics of Aerosolized Tobramycin in Adults with Cystic Fibrosis. The Journal of Clinical Pharmacology. 34:255-259 (1994).
32. M. Hoppentocht, P. Hagedoorn, H.W. Frijlink, and A.H. de Boer. Developments and strategies for inhaled antibiotic drugs in tuberculosis therapy: A critical evaluation. European Journal of Pharmaceutics and Biopharmaceutics. 86:23-30 (2014).
33. S. Stanojevic, V. Waters, J.L. Mathew, L. Taylor, and F. Ratjen. Effectiveness of inhaled

tobramycin in eradicating Pseudomonas aeruginosa in children with cystic fibrosis. Journal of Cystic Fibrosis. 13:172-178 (2014).
34. D.E. Geller, W.H. Pitlick, P.A. Nardella, W.G. Tracewell, and B.W. Ramsey. PHarmacokinetics and bioavailability of aerosolized tobramycin in cystic fibrosis. Chest. 122:219-226 (2002).
35. M.B. Dolovichand R. Dhand. Aerosol drug delivery: developments in device design and clinical use. The Lancet. 377:1032-1045.
36. B.M. Ibrahim, M.D. Tsifansky, Y. Yang, and Y. Yeo. Challenges and advances in the development of inhalable drug formulations for cystic fibrosis lung disease. Expert Opinion on Drug Delivery. 8:451-466 (2011).
37. A. Kuzmovand T. Minko. Nanotechnology approaches for inhalation treatment of lung diseases. J Control Release.
38. D. T, M. N, and W. P. Nebuliser systems for drug delivery in cystic fibrosis. Cochrane Database of Systematic Reviews(2013).
39. B.C. Tang, M. Dawson, S.K. Lai, Y.-Y. Wang, J.S. Suk, M. Yang, P. Zeitlin, M.P. Boyle, J. Fu, and J. Hanes. Biodegradable polymer nanoparticles that rapidly penetrate the human mucus barrier. Proceedings of the National Academy of Sciences. 106:19268-19273 (2009).
40. S. Stegemann, S. Kopp, G. Borchard, V.P. Shah, S. Senel, R. Dubey, N. Urbanetz, M. Cittero, A. Schoubben, C. Hippchen, D. Cade, A. Fuglsang, J. Morais, L. Borgström, F. Farshi, K.H. Seyfang, R. Hermann, A. van de Putte, I. Klebovich, and A. Hincal. Developing and advancing dry powder inhalation towards enhanced therapeutics. European Journal of Pharmaceutical Sciences. 48:181-194 (2013).
41. A.B. Wattsand R.O. Williams. Nanoparticles for Pulmonary Delivery. In D.C.H. Smythand J.A. Hickey (eds.), Controlled Pulmonary Drug Delivery, Springer New York, New York, NY, 2011, pp. 335-366.
42. E.-M. Collnot, C. Baldes, M.F. Wempe, J. Hyatt, L. Navarro, K.J. Edgar, U.F. Schaefer, and C.-M. Lehr. Influence of vitamin E TPGS poly(ethylene glycol) chain length on apical efflux transporters in Caco-2 cell monolayers. J Control Release. 111:35-40 (2006).
43. S.A. Meenach, K.W. Anderson, J. Zach Hilt, R.C. McGarry, and H.M. Mansour. Characterization and aerosol dispersion performance of advanced spray-dried chemotherapeutic PEGylated phospholipid particles for dry powder inhalation delivery in lung cancer. European Journal of Pharmaceutical Sciences. 49:699-711 (2013).
44. F. W. The ARLA Respiratory Deposition Calculator2008.
45. O. Mert, S.K. Lai, L. Ensign, M. Yang, Y.-Y. Wang, J. Wood, and J. Hanes. A poly(ethylene glycol)-based surfactant for formulation of drug-loaded mucus penetrating particles. J Control Release. 157:455-460 (2012).
46. A. Bootz, V. Vogel, D. Schubert, and J. Kreuter. Comparison of scanning electron microscopy, dynamic light scattering and analytical ultracentrifugation for the sizing of poly(butyl cyanoacrylate) nanoparticles. European Journal of Pharmaceutics and

Biopharmaceutics. 57:369-375 (2004).
47. S.A. Meenach, Y.J. Kim, K.J. Kauffman, N. Kanthamneni, E.M. Bachelder, and K.M. Ainslie. Synthesis, Optimization, and Characterization of Camptothecin-Loaded Acetalated Dextran Porous Microparticles for Pulmonary Delivery. Molecular Pharmaceutics. 9:290-298 (2012).
48. X. Wu, D. Hayes, J.B. Zwischenberger, R.J. Kuhn, and H.M. Mansour. Design and physicochemical characterization of advanced spray-dried tacrolimus multifunctional particles for inhalation. Drug Design, Development and Therapy. 7:59-72 (2013).
49. S.A. Meenach, F.G. Vogt, K.W. Anderson, J.Z. Hilt, R.C. McGarry, and H.M. Mansour. Design, physicochemical characterization, and optimization of organic solution advanced spray-dried inhalable dipalmitoylphosphatidylcholine (DPPC) and dipalmitoylphosphatidylethanolamine poly(ethylene glycol) (DPPE-PEG) microparticles and nanoparticles for targeted respiratory nanomedicine delivery as dry powder inhalation aerosols. International Journal of Nanomedicine. 8:275-293 (2013).
50. X. Wu, W. Zhang, D. Hayes, and H.M. Mansour. Physicochemical characterization and aerosol dispersion performance of organic solution advanced spray-dried cyclosporine A multifunctional particles for dry powder inhalation aerosol delivery. International Journal of Nanomedicine. 8:1269-1283 (2013).
51. X. Liand H.M. Mansour. Physicochemical Characterization and Water Vapor Sorption of Organic Solution Advanced Spray-Dried Inhalable Trehalose Microparticles and Nanoparticles for Targeted Dry Powder Pulmonary Inhalation Delivery. AAPS PharmSciTech. 12:1420-1430 (2011).
52. A.J. Hickey, H.M. Mansour, M.J. Telko, Z. Xu, H.D.C. Smyth, T. Mulder, R. McLean, J. Langridge, and D. Papadopoulos. Physical characterization of component particles included in dry powder inhalers. I. Strategy review and static characteristics. Journal of Pharmaceutical Sciences. 96:1282-1301 (2007).
53. C. Nora Y.K. , Hak-Kim Chan. The Role of Particle Properties in Pharmaceutical Powder Inhalation Formulations. Journal of Aerosol Medicine. 15:325-330 (2002).
54. G. Mohammadi, H. Valizadeh, M. Barzegar-Jalali, F. Lotfipour, K. Adibkia, M. Milani, M. Azhdarzadeh, F. Kiafar, and A. Nokhodchi. Development of azithromycin–PLGA nanoparticles: Physicochemical characterization and antibacterial effect against Salmonella typhi. Colloids and Surfaces B: Biointerfaces. 80:34-39 (2010).
55. W. Kaialyand A. Nokhodchi. Dry powder inhalers: Physicochemical and aerosolization properties of several size-fractions of a promising alterative carrier, freeze-dried mannitol. European Journal of Pharmaceutical Sciences. 68:56-67 (2015).
56. Z. Zhang, L. Xu, H. Chen, and X. Li. Rapamycin-loaded poly(ε-caprolactone)-poly(ethylene glycol)-poly(ε-caprolactone) nanoparticles: preparation, characterization and potential application in corneal transplantation. Journal of Pharmacy and Pharmacology. 66:557-563 (2014).
57. X. Li, S. Chang, G. Du, Y. Li, J. Gong, M. Yang, and Z. Wei. Encapsulation of azithromycin into polymeric microspheres by reduced pressure-solvent evaporation

method. International Journal of Pharmaceutics. 433:79-88 (2012).
58. F. Ungaro, G. De Rosa, A. Miro, F. Quaglia, and M.I. La Rotonda. Cyclodextrins in the production of large porous particles: Development of dry powders for the sustained release of insulin to the lungs. European Journal of Pharmaceutical Sciences. 28:423-432 (2006).
59. S. Sand H. AJ. Drug properties affecting aerosol behavior. Respiratory Care. 45:652-666 (2000).
60. H. AJand M. HM. Delivery of drugs by the pulmonary route, Taylor and Francis, New York, 2009.
61. A.J. Hickeyand H.M. Mansour. Formulation challenges of powders for the delivery of small molecular weight molecules as aerosols, Informa Healthcare, New York, 2008.
62. D.A. Edwards. The macrotransport of aerosol particles in the lung: Aerosol deposition phenomena. Journal of Aerosol Science. 26:293-317 (1995).

TABLES AND FIGURES

Table 1. Size (as measured by dynamic light scattering), polydispersity index (PDI), zeta potential (ζ), drug loading, and encapsulation efficiency (EE) of nanoparticles (mean ± standard deviation, n = 3).

NP System	Diameter (nm)	PDI	ζ Potential (mV)	Drug Loading (mg drug/100mg NP)	EE (%)
AZI-NP	204.7 ± 0.4	0.11 ± 0.01	-4.62 ± 0.19	3.89 ± 2.67	13.0 ± 0.9
RAP-NP	189.1 ± 1.1	0.16 ± 0.02	-2.26 ± 0.14	2.58 ± 0.04	25.8 ± 0.4
Blank	211.4 ± 3.2	0.18 ± 0.03	-6.13 ± 0.62	n/a	n/a

Table 2. Size (as measured by SEM imaging and ImageJ analysis), water content, drug loading, nanoparticle (NP) loading in nanocomposite microparticles (nCmP), and NP loading efficacy in nCmP (mean ± standard deviation, n = 3).

nCmP System	Diameter (μm)	Water Content (%)	Drug Loading (mg drug/100 mg nCmP)	NP Loading (%)	NP Loading Efficacy (%)
AZI-nCmP	1.03 ± 0.46	5.7 ± 1.25	0.77 ± 0.08	20.47 ± 1.80	40.94 ± 3.60
RAP-nCmP	1.12 ± 0.43	6.1 ± 1.05	0.56 ± 0.02	20.14 ± 0.68	44.28 ± 1.34

Table 3. *In vitro* aerosol dispersion performance properties including mass median aerodynamic diameter (MMAD), geometric standard deviation (GSD), fine particle dose (FPD), fine particle fraction (FPF), respirable fraction (RF), and emitted dose (ED) for nCmP (mean ± standard deviation, n = 3).

nCmP system	MMAD (μm)	GSD (μm)	FPD (mg)	FPF (%)	RF (%)	ED (%)
AZI-nCmP	3.93 ± 0.09	1.73 ± 0.06	19.63 ± 0.59	93.9 ± 1.3	79.7 ± 0.8	98.9 ± 0.4
RAP-nCmP	3.86 ± 0.07	1.78 ± 0.06	20.90 ± 0.62	92.5 ± 1.7	73.6 ± 2.1	99.7 ± 0.3

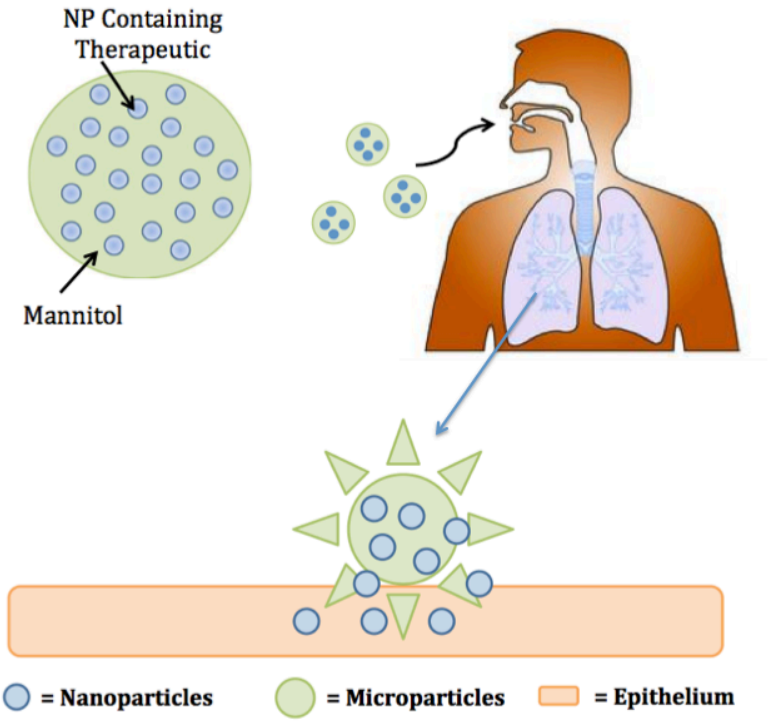

Figure 1. Schematic of an aerosol nanoparticle microparticle (nCmP) system interacting with the pulmonary mucosa. Once the nCmP impact the surface of the mucus coating the pulmonary epithelium they immediately degrade to release nanoparticles.

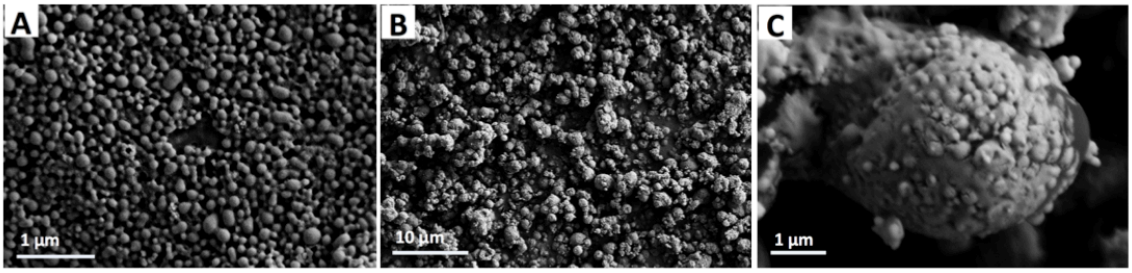

Figure 2. Representative SEM micrographs of azithromycin (AZI) nanoparticles (NP) and nanocomposite microparticles (nCmP) including: (A) AZI-NP, (B) AZI-nCmP, (C) Representative zoomed in image of AZI-nCmP.

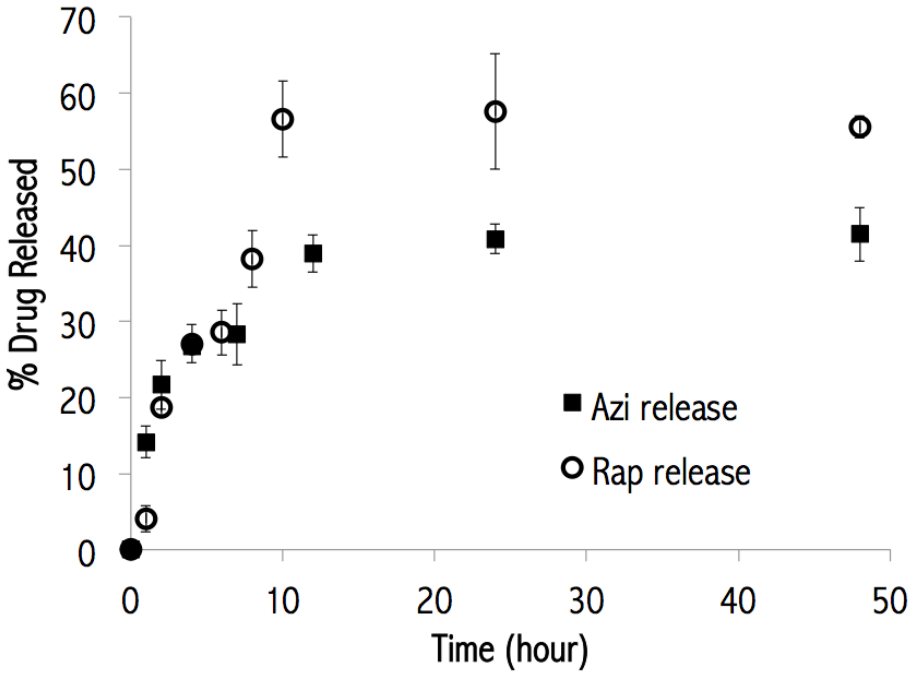

Figure 3. *In vitro* drug release profiles for azithromycin (AZI) and rapamycin (RAP) nanoparticle systems.

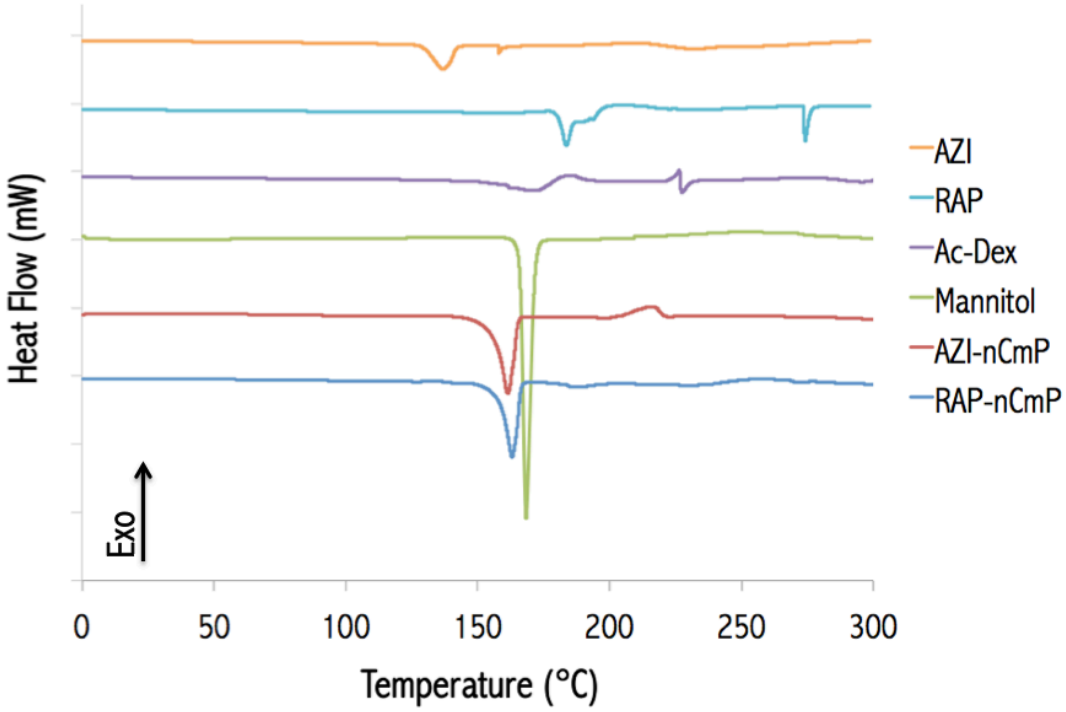

Figure 4. Differential scanning calorimetry (DSC) thermograms of raw azithromycin (AZI), raw rapamycin (RAP), raw acetalated dextran (Ac-Dex), raw mannitol, AZI-nCmP, and RAP-nCmP.

720

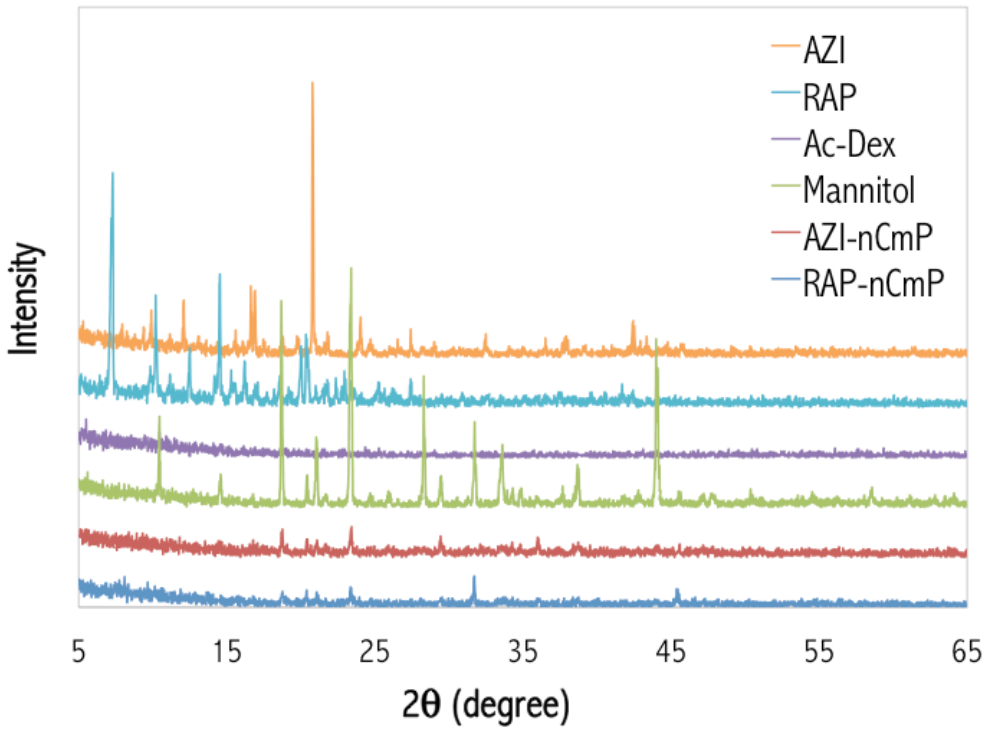

721

722 **Figure 5**. Powder X-ray (PXRD) diffractograms of raw azithromycin (AZI), raw rapamycin
723 (RAP), raw acetalated dextran (Ac-Dex), raw mannitol, AZI-nCmP, and RAP-nCmP.

724

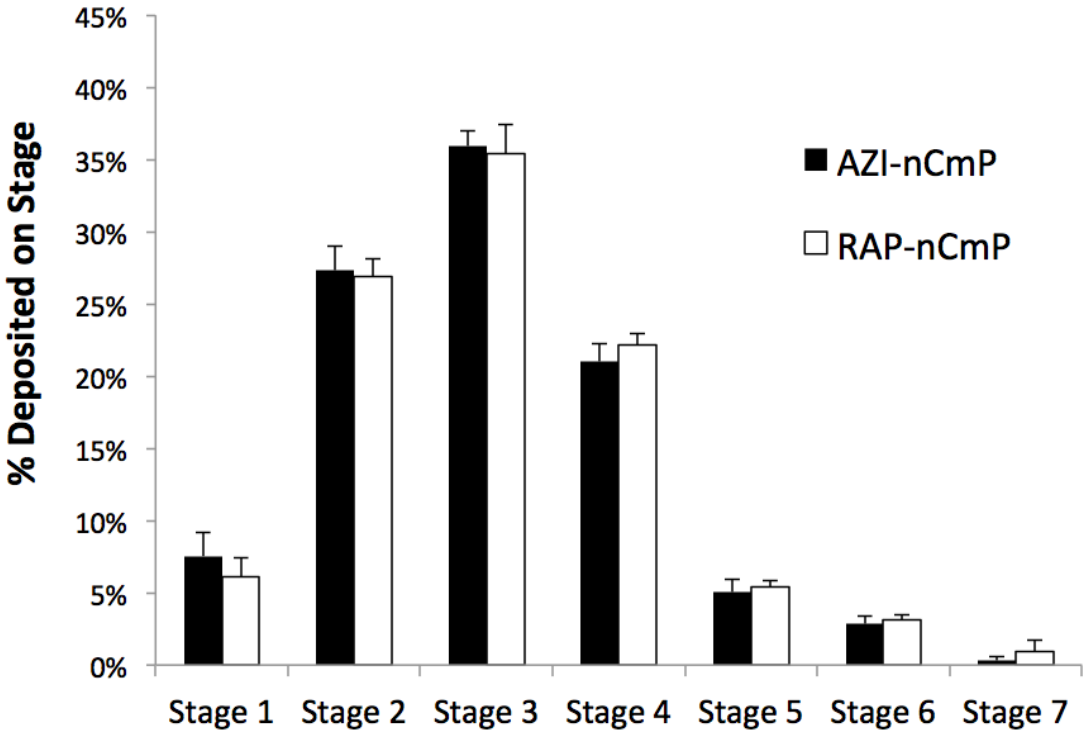

Figure 6. Aerosol dispersion performance as % deposited on each stage of the Next Generation Impactor™ (NGI™) for AZI- and RAP-nCmP.

SUPPLEMENTARY MATERIAL

Table S1. Characterization of nanoparticles after redispersion from nanocomposite microparticles in PBS including the size, polydispersity index (PDI), and zeta (ζ) potential.

System	Diameter (nm)	PDI	ζ Potential (mV)
AZI-NP	327.6 ± 3.7	0.32 ± 0.02	-7.66 ± 0.68
RAP-NP	348.2 ± 11.6	0.43 ± 0.01	-5.99 ± 0.07
Blank-NP	270.8 ± 10.8	0.26 ± 0.04	-3.98 ± 0.67

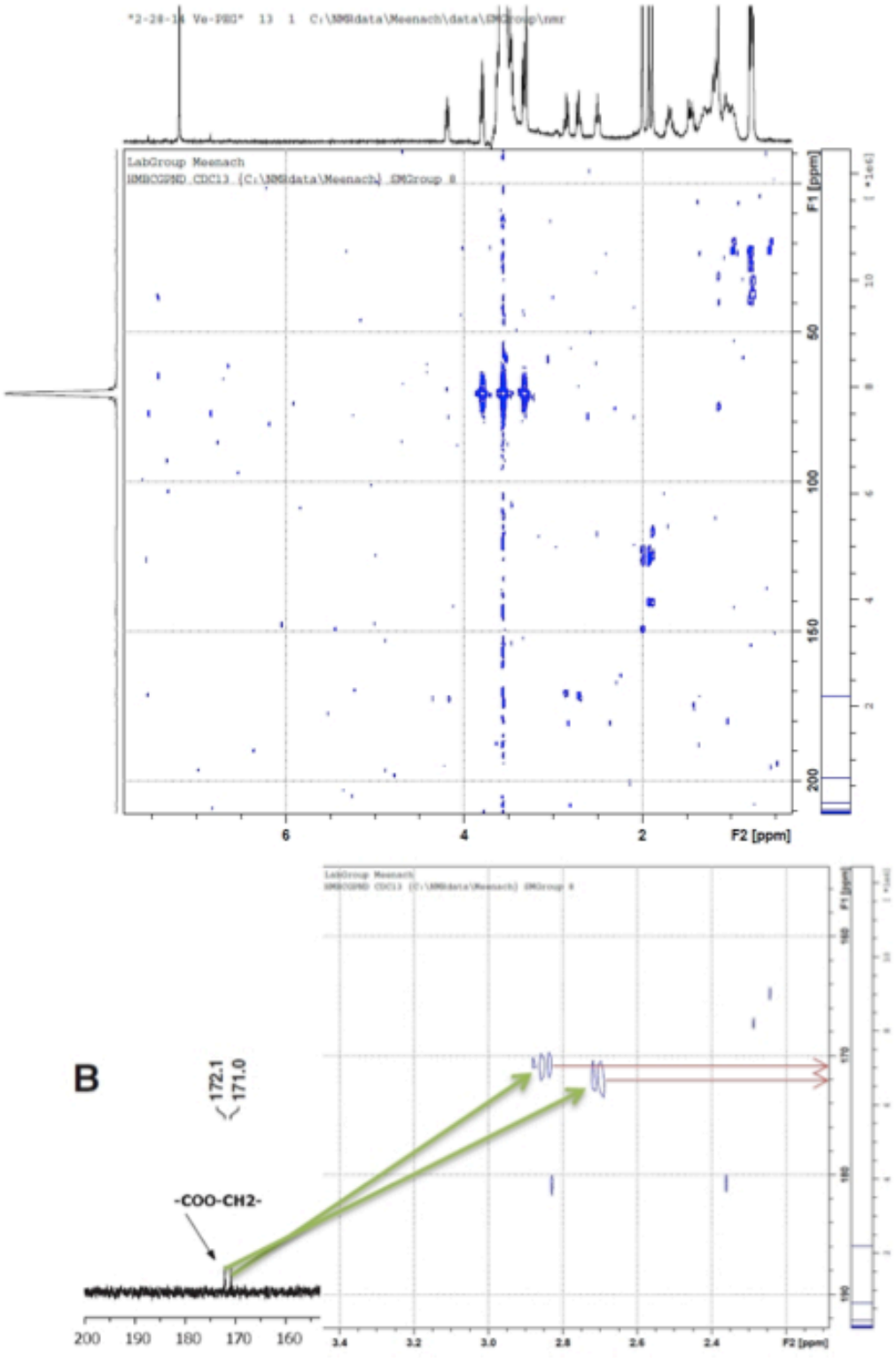

Figure S1. NMR spectra where (top) indicates entire spectra and (bottom) is an enlarged portion.